Experimental Mechanics (2010) 50:169–177
DOI 10.1007/s11340-009-9317-7

Residual Stress Determination Using Cross-Slitting and Dual-Axis ESPI

G.S. Schajer · Y. An

Received: 25 June 2009 / Accepted: 9 November 2009 / Published online: 12 December 2009

Abstract Hole-drilling and Electronic Speckle Pattern Interferometry (ESPI) are used to measure residual stresses in metal specimens. The slitting method is chosen as an alternative to the more commonly used hole-drilling method because it involves less material removal and leaves large areas of highly deformed material available to be measured. However the conventional single-slitting method is sensitive only to the stress component perpendicular to the slit direction, and thus has a strong directional bias. Conventional ESPI has a similar bias because it responds to surface displacements in a specific sensitivity direction. In this paper, a novel cross-slitting method with dual-axis ESPI measurements is proposed to address both directional biases. Cross-slitting is introduced as a means of releasing all in-plane stress components. The dual-axis ESPI system uses diagonal-mirror and shutter devices to provide surface displacement measurements in orthogonal in-plane directions. The combination of the cross-slit and dual-axis measurement gives isotropic sensitivity to the in-plane residual stress components. Experimental measurements are described that illustrate the capability and effectiveness of the cross-slitting/ESPI technique.

Keywords Residual stress measurement · ESPI · Slitting · Hole-drilling · Inverse calculations

Presented at the SEM Annual Conference and Exposition, Albuquerque, NM, June 1–4, 2009.

G.S. Schajer (✉, SEM member) · Y. An (SEM member)
Department of Mechanical Engineering,
University of British Columbia,
Vancouver V6T 1Z4, Canada
e-mail: schajer@mech.ubc.ca

Introduction

The strain gauge hole-drilling method [1, 2] is one of the most widely used techniques for measuring residual stresses. It is practical, reliable and causes relatively small damage to the test specimen. However, the installation of strain gauges and associated wiring is very time consuming. The amount of available data is also limited. For every measurement, only three discrete readings are available, just sufficient to evaluate the three in-plane residual stresses.

Electronic Speckle Pattern Interferometry (ESPI) [3, 4] provides additional opportunities for measuring surface displacements for hole-drilling residual stress evaluations [5, 6]. The non-contact nature of the technique avoids the significant time taken to install strain gages, associated wiring and surface coating. In addition, ESPI provides a much richer, full-field data set than is available from strain gauges. However, hole-drilling involves removal of the most data-rich part of the specimen, the material within the hole. It is possible to reduce this loss of data-rich material by cutting a narrow slit [7, 8] instead of a circular hole. Significant areas of highly deformed material then remain adjacent to the edges of the slit. However a single slit can only relieve normal stresses perpendicular to the slit and the shear stresses. Thus, it can only indicate up to two of three in-plane stress components, and so creates a biased estimation.

Typical ESPI systems use a single axis illumination, which allows the method to give a single directional displacement measurement. This single directional measurement is a further source of biased estimation

This paper presents a novel cross-slitting method with dual-axis ESPI measurements. The proposed method

combines the advantages of ESPI and the slitting method. It gathers a rich source of data and overcomes the directional measurement biases by cross-slitting and measuring two orthogonal displacement maps. The effectiveness of this method is examined by doing example measurements in a specimen containing known residual stresses.

Cross-slitting Method

Figure 1(a) illustrates the single slitting method [7, 8]. A slit is cut in the specimen and the resulting deformations are typically measured using strain gauges attached to the upper and/or lower surfaces. However, only stresses perpendicular to the slit face, σ_x, τ_{xy}, are released and can be calculated from the strain measurements. To overcome this limitation and get a full evaluation of all the in-plane stress components, a new cross-slitting method is proposed.

Figure 1(b) illustrates the proposed cross-slitting method. Two perpendicular slits are cut into the surface, vertical slit 1 releases in-plane residual stress components σ_x, τ_{xy}, and horizontal slit 2 releases σ_y and τ_{xy}. The length of the slits determines the capability of the method to determine subsurface stresses. Stresses down to about half the slit length can be evaluated. For conventional hole drilling, the equivalent circular hole shown in Fig. 1(c) would have a diameter equal to the slit length and would also allow subsurface stress evaluation down to about half its diameter.

Ideally, the slit width would be very small to maximize the four adjacent areas of highly deformed material around the slit intersection. These data-rich areas contain high surface deformations that greatly enhance the accuracy of cross-slitting measurements. They are lost during hole drilling using the equivalent circular hole shown in Fig. 1(c). In practice, the slit width has a moderate size because it must be cut using an endmill. Typical endmills have a cutting length four times their diameter. Thus, if they are to reach a depth equal to half the slot length, the slot width must equal one eighth of its length.

Electronic Speckle Pattern Interferometry

Figure 2 shows an Electronic Speckle Pattern Interferometry (ESPI) arrangement for in-plane displacement measurements. In this arrangement, the light from a laser source is divided by a beam splitter into two halves, one becoming a reference beam and the other an illumination beam. After reflection from mirrors, both beams interfere at the surface of the test specimen. A CCD camera images and records the resulting interference (speckle) pattern. The surface deformations caused by slitting are evaluated by subtracting the phase maps measured before and after slitting. These phase maps are evaluated by measuring sets of speckle patterns with 90° phase steps introduced into the reference beam by a piezo actuator behind one mirror [4]. For the arrangement shown in Fig. 2, the displacement sensitivity vector is in the plane of the specimen surface and perpendicular to the adjacent mirror. The optical arrangement shown differs from conventional in-plane ESPI systems by the use of this adjacent mirror. It enables the illumination and reference beams to be close to each other over most of their span, thereby improving ESPI measurement stability by the sharing of an "almost" common path [9].

A typical limitation of the conventional single axis ESPI technique is that it measures surface displacement components only in the one specific sensitivity direction. This feature causes a bias in residual stress measurements because the associated displacement components derive mostly from the parallel in-plane stress. The perpendicular in-plane stress produces much smaller displacements in the sensitivity direction, mostly due to the action of Poisson's ratio.

Figure 3 illustrates the residual stress measurement bias. The diagram shows the single-axis ESPI fringes theoretically expected for axial stresses of 100 MPa in aluminum. Figure 3(a) shows the expected fringes for a surface stress parallel to the sensitivity direction. Six fringes extending over a large area are created. Figure 3(b) shows the expected fringes for a surface stress perpendicular to the sensitivity direction. The associated displacements derive solely from Poisson's ratio effects, and only two localized

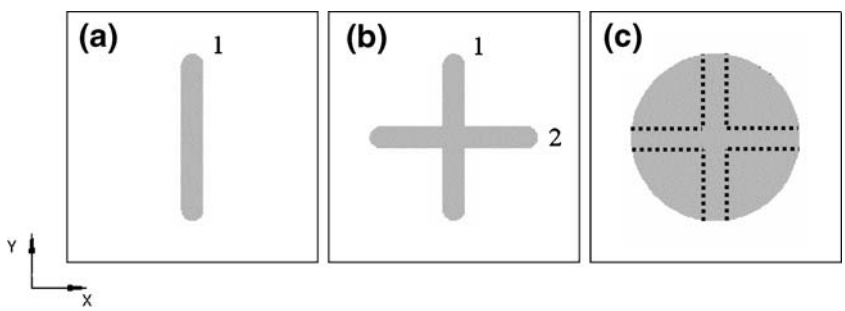

Fig. 1 Single and cross-slitting: (**a**) Single slit, (**b**) Cross slits, (**c**) Circular hole

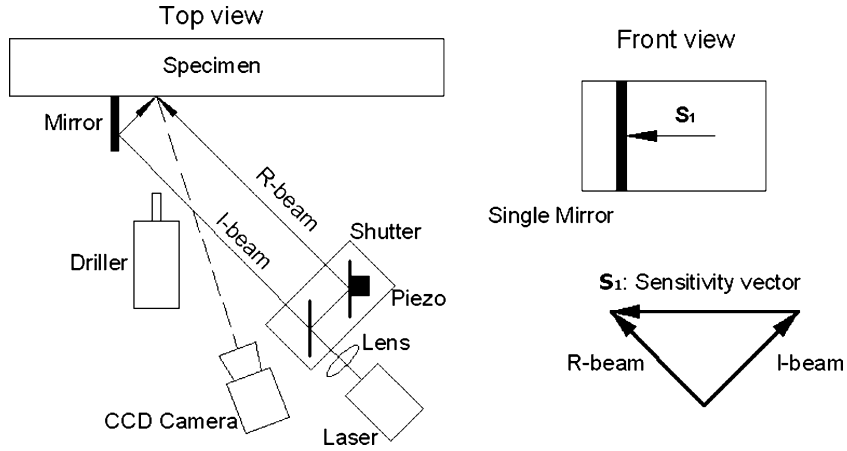

Fig. 2 Schematic arrangement of in-plane ESPI measurement

fringes are formed. This small response significantly impairs the accuracy and reliability of the perpendicular stress evaluation.

Dual-axis ESPI Technique

A novel dual-axis ESPI system is presented here that is capable of making displacement measurements in two perpendicular directions. This arrangement eliminates the measurement bias inherent in single-axis ESPI measurements.

Figure 4 shows the proposed dual-axis ESPI system. This optical arrangement is a generalization of the single-axis system shown in Fig. 2. Light from the laser is divided by beam splitters into three switchable parts. The first part goes to the lower of a pair of diagonal mirrors and is reflected to the specimen surface. The second part goes to the upper mirror and is also reflected to the specimen. The third part acts as a reference beam. It illuminates the specimen surface after reflection from a mirror attached to a piezo actuator. This actuator steps the length of the reference beam by quarter wavelength intervals to enable use of the phase stepping method [10]. By controlling some shutters, the lower and upper mirrors can be illuminated separately. The two sensitivity vectors for the dual-axis ESPI system can be identified from Fig. 5. In the plan view, all beams are (approximately) parallel, with reflection angle θ. The reference beam has vector direction $\mathbf{k_0}$, while the illumination beams have vector directions $\mathbf{k_1}$ and $\mathbf{k_2}$ after reflection from the diagonal mirrors.

For diagonal mirrors that are perpendicular to the specimen surface in the plan view and ±45° in the front view, the sensitivity vector in direction 1 (using the lower mirror) is:

$$\mathbf{S_1} = \mathbf{k_0} - \mathbf{k_1} = -\sin\theta(\mathbf{i} + \mathbf{j}) \tag{1}$$

and for direction 2 (using the upper mirror) is:

$$\mathbf{S_2} = \mathbf{k_0} - \mathbf{k_2} = -\sin\theta(\mathbf{i} - \mathbf{j}) \tag{2}$$

where θ is the reflection angle and **i**, **j** are the unit vectors in the x and y directions. The two sensitivity directions $\mathbf{S_1}$ and $\mathbf{S_2}$ are orthogonal, thereby balancing the calculation sensitivity for the in-plane normal stresses and making the residual stress evaluation more accurate overall.

The phase shift change measured using the ESPI technique is:

$$\Delta\varphi = (2\pi/\lambda)\mathbf{S_x} \cdot \mathbf{d} \tag{3}$$

where a 5-step phase stepping procedure [10] is used here to evaluate phase change. By subtracting the phase maps measured before and after slitting, "wrapped" phase maps, i.e., with modulo 2π discontinuities are obtained. The discontinuities can be removed mathematically to produce unwrapped phase maps [11], from which the displacements in the two sensitivity directions can be determined.

Residual Stress Calculation

The relationship between the measured displacement data and the residual stresses for the slitting method has the form of an integral equation [12]:

$$\mathrm{d(h)} = \frac{1}{\mathrm{E}} \int_0^{\mathrm{h}} \mathrm{g(H,h)}\ \sigma(\mathrm{H})\ \mathrm{dH} \qquad 0 \le \mathrm{H} \le \mathrm{h} \tag{4}$$

where d(h) are the measured displacements when the slit is cut to a depth h. The stresses σ(H) act perpendicularly to the slit, and are uniform over the length of the slit.[1] The kernel function g(H,h) describes the displacement response due to a unit stress at depth H within a slit of depth h. This function depends on the geometry of the slits and the specimen. Equation (4) shows that the displacement d(h) depends on the combination of stresses σ(H) at all depths H

[1] In a recently published paper, Montay et al. [13] presented an interesting ESPI procedure where subsurface stresses were determined for the case of non-uniform stresses along the length of a single slot.

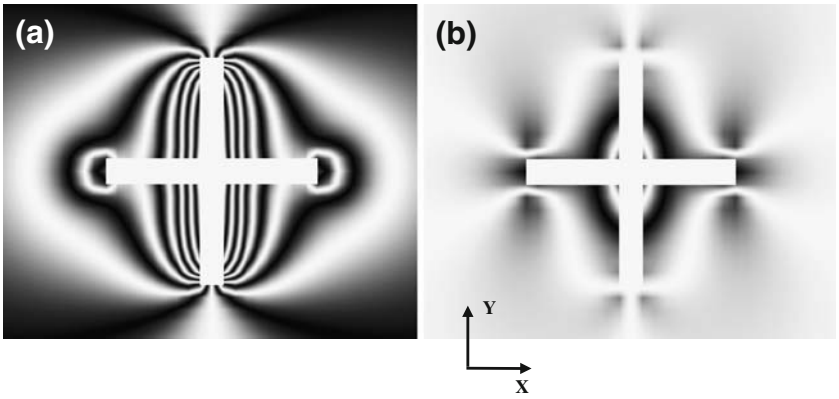

Fig. 3 Synthetic fringes for sensitivity in the x-direction: (**a**) σ_x=100 MPa, (**b**) σ_y=100 MPa. Material = alumimum, E= 70 GPa, slot length=12.7 mm, slot depth=6.35 mm

within the slit depth h. The equation is an "inverse problem" [14] because the stresses σ(H) to be determined are within the integral, while the measured displacement data are outside.

The stress vs. depth profile σ(H) can be estimated by making surface displacement measurements after each of a series of increments in slit depth [12]. If the stresses within each depth increment are assumed to be uniform, then equation (4) can be rewritten in matrix form:

$$\mathbf{G}\,\mathbf{m} = \mathbf{d} \tag{5}$$

where **m** is a vector containing the stresses within each depth increment and **d** is a vector containing the displacements at each slit depth. The matrix components G_{ij} represent the displacements caused by a unit uniform stress within increment "j" of a slit "i" increments deep. For 5 depth increments, equation (5) becomes:

$$\begin{bmatrix} G_{11} & & & & \\ G_{21} & G_{22} & & & \\ G_{31} & G_{32} & G_{33} & & \\ G_{41} & G_{42} & G_{43} & G_{44} & \\ G_{51} & G_{52} & G_{53} & G_{54} & G_{55} \end{bmatrix} \begin{bmatrix} m_1 \\ m_2 \\ m_3 \\ m_4 \\ m_5 \end{bmatrix} = \begin{bmatrix} d_1 \\ d_2 \\ d_3 \\ d_4 \\ d_5 \end{bmatrix} \tag{6}$$

Figure 6 illustrates a physical interpretation of matrix **G**. The figure shows that only stresses that are within the slit depth contribute to the surface deformations. Thus, matrix **G** is lower triangular.

In practical calculations, each element in equation (6) represents a group of quantities. Element m_j of the stress solution is a vector of nine quantities $(\sigma_x\ \sigma_y\ \tau_{xy}\ \omega_1\ \omega_2\ \omega_3\ \omega_4\ \omega_5\ \omega_6)^T$. The first three quantities are the Cartesian stresses within the depth increment j. The second three quantities are the rigid-body motions (one translation and two rotations) of the specimen observed in measurements in sensitivity direction 1. The third three quantities are the rigid-body motions observed in measurements in sensitivity direction 2. The various "rigid-body motions" also include additional measurement artifacts induced by local variations in air temperature within the beam paths. These combined motions tend to degrade the measured data, and they appear in equation (6) only as a means of removing their effects from the stress calculation [6]. Their calculated values do not relate to residual stresses.

Similarly, element d_i in equation (6) represents a vector of quantities comprising the measurements of all the pixel phases measured using the upper mirror, followed by all the pixel phases measured using the lower mirror. Correspondingly, matrix **G** has a block lower triangular structure where each block has the form:

$$\mathbf{G}_{ij} = \begin{array}{c} \begin{matrix} \sigma_x & \sigma_y & \tau_{xy} & \omega_1 & \omega_2 & \omega_3 & \omega_4 & \omega_5 & \omega_6 \end{matrix} \\ \left[\begin{array}{ccc:ccc:ccc} \times & \times & \times & \times & \times & \times & 0 & 0 & 0 \\ \times & \times & \times & \times & \times & \times & 0 & 0 & 0 \\ \times & \times & \times & \times & \times & \times & 0 & 0 & 0 \\ \hdashline \times & \times & \times & 0 & 0 & 0 & \times & \times & \times \\ \times & \times & \times & 0 & 0 & 0 & \times & \times & \times \\ \times & \times & \times & 0 & 0 & 0 & \times & \times & \times \end{array}\right] \end{array} \tag{7}$$

Sensitivity direction 2

Sensitivity direction 1

Each block contains nine columns corresponding to the components of m_j, and rows corresponding to the sum of the number of active pixels in the two sensitivity directions (only three typical rows are shown for each sensitivity direction). The first three columns of G_{ij}, corresponding to the stresses, are computed using finite element calculations. The upper half of the next three columns correspond to the apparent rigid-body motions observed in sensitivity direction 1, and the lower half of the last three columns correspond to these motions observed in sensitivity direction 2. The unused half columns contain zeroes.

When expressed in fully expanded form, matrix **G** in equation (5) is very large, with several tens of columns and many hundreds of thousands of rows, causing the

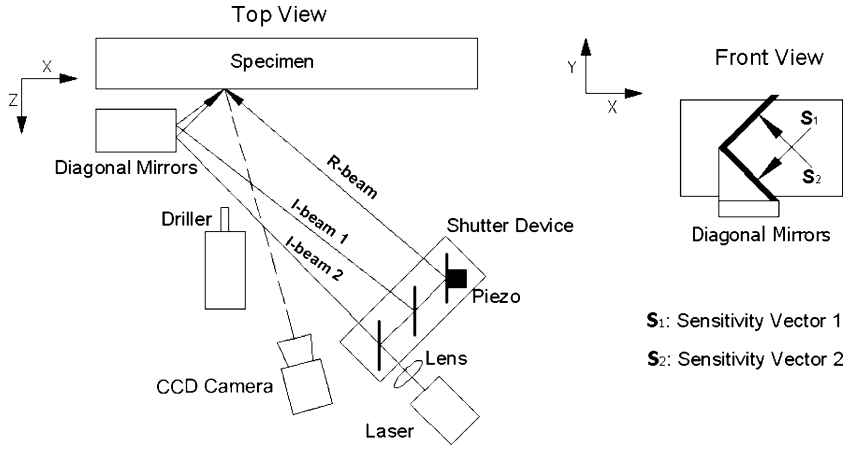

Fig. 4 Dual-axis ESPI system

resulting matrix equation to be highly over-determined. The equation may be solved in the least-squares sense using [14]:

$$\left(\mathbf{G}^{\mathbf{T}}\mathbf{G}\right)\mathbf{m} = \mathbf{G}^{\mathbf{T}}\mathbf{d} \tag{8}$$

Matrix $\mathbf{G}^{\mathbf{T}}\mathbf{G}$ and vector $\mathbf{G}^{\mathbf{T}}\mathbf{d}$ are of relatively modest size, with only some tens of columns and rows. If some care is taken with the sequence of the summations done when pre-multiplying by $\mathbf{G}^{\mathbf{T}}$, it is possible to avoid having to form matrix $\mathbf{G}$ explicitly. Instead, one may work directly from finite-element computed deformation maps such as were used to evaluate Fig. 3. Some further computational economy can be achieved by noting that matrix $\mathbf{G}^{\mathbf{T}}\mathbf{G}$ is symmetrical.

Figure 7 shows some details of the finite element mesh [15] used for calculating the displacement responses contained in the first three columns of equation (7). With consideration of the symmetric geometry, one-quarter models with various cutting depths can be used. These models are capable of calculating displacement responses separately for all three stress-states by appropriately changing the loads and boundary conditions. A rectangular mesh pattern was chosen for the area around the cross-slits to simplify interpolation of the displacement data at each point on the top surface corresponding to the measured pixels.

Experimental Results

A test specimen made from a T6061-T4 aluminum plate, 8″×4″ (203×102 mm) and 0.5″ (12.7 mm) thick was used to demonstrate the cross-slitting/ESPI technique. Known residual stresses were created by loading the plate in a four-point bending fixture and monitoring the applied load and the surface strains in the central section as the load was increased substantially into the plastic range and then removed. The plastic deformation during loading followed

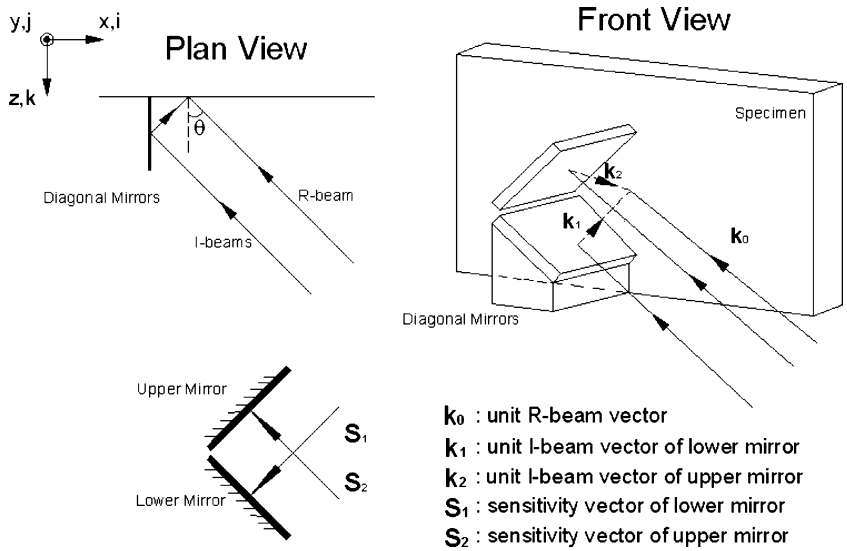

Fig. 5 Diagonal-mirror assembly and sensitivity vectors

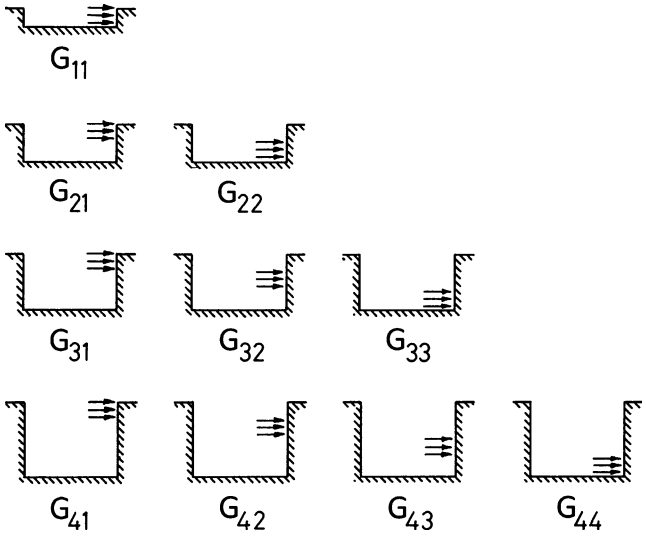

Fig. 6 Physical interpretation of matrix coefficients for the slitting method (adapted from Schajer and Prime [12])

by elastic unloading created an in-plane residual stress profile within the specimen. This profile could be determined from the uniaxial stress-strain curve computed from the bending load and surface strain data [16, 17]. In this case, where the beam specimen was a wide plate, the central portion underwent plane strain deformation. Consequently, transverse stresses were also created, ν times the longitudinal stresses.

An initial reference set of stepped images was recorded in the two sensitivity directions before any slitting. A 25,000 rpm electric drill with a $^1/_{16}$″ (1.59 mm) diameter 2-flute milling cutter was then used to cut the cross-slits. The drill was attached on a 3-axis translation stage, thereby creating a miniature milling machine. Cross-slits 0.5″ (12.7 mm) long were cut in five depth increments of 0.050″ (1.27 mm) to a maximum depth of 0.250″ (6.35 mm). After each depth increment, a further set of stepped images was recorded in each sensitivity direction. The corresponding phase maps were evaluated using a five-step phase identification algorithm [10]. To minimize the time between the reference and subsequent phase maps, each phase map was used as the reference for the next depth increment. This practice improved correlation between images and thereby improved the resulting fringe image quality. Using this approach, the measured fringes represented the incremental changes in the surface displacements. To accommodate this arrangement in the residual stress calculations, each block of rows in matrix **G** was modified by subtracting the previous block of rows. Before proceeding with the residual stress calculations, the phase maps corresponding to all the incremental depth increases were unwrapped [11] to eliminate modulo 2π phase discontinuities.

Figure 8 shows the five incremental ESPI fringe patterns measured in sensitivity direction 1. The diagonal tilt of the fringe patterns reflects the 45° tilt of the sensitivity direction 1. The opposite diagonal tilt occurs in the fringes measured in sensitivity direction 2. The illustrated fringes have several desirable features: 1) they are well-defined, indicating good image quality, 2) they are numerous, indicating a high sensitivity, and 3) they have distinctly different shapes, enabling the inverse calculation to separate the various stress components well.

Figure 9(a) shows the stress profiles calculated from the dual-axis ESPI cross-slitting measurements using equation (8). This graph illustrates the stresses within half the specimen thickness. The bending-induced residual stresses are compressive at the surface (depth=0), linearly changing to a tensile peak at 4–5 mm depth, and then reducing to zero at the neutral plane at 6.35 mm depth. As expected, the normal stresses σ_x (parallel to the original bending loading) are the largest. The normal stresses σ_y are about one third of the σ_x stresses due to the action of Poisson's ratio in plane-strain bending. The shear stresses τ_{xy} are close to zero because of symmetry. Similar ESPI/cross-slitting

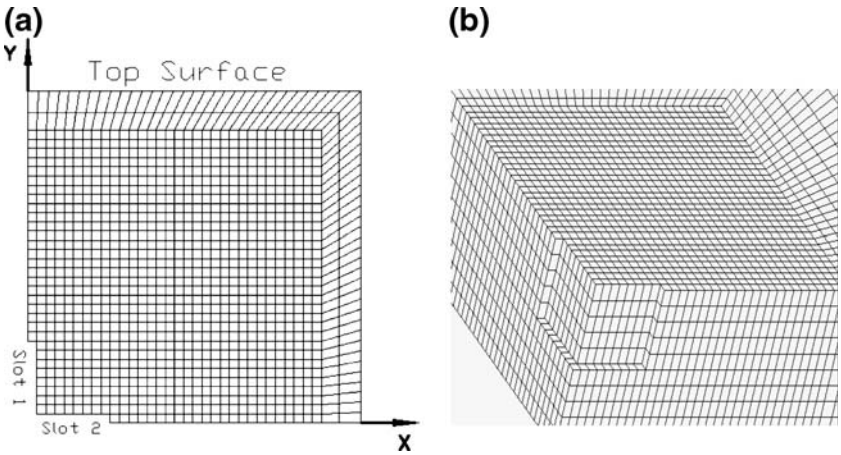

Fig. 7 Details of the finite element model: (**a**) Top surface view, (**b**) Side view

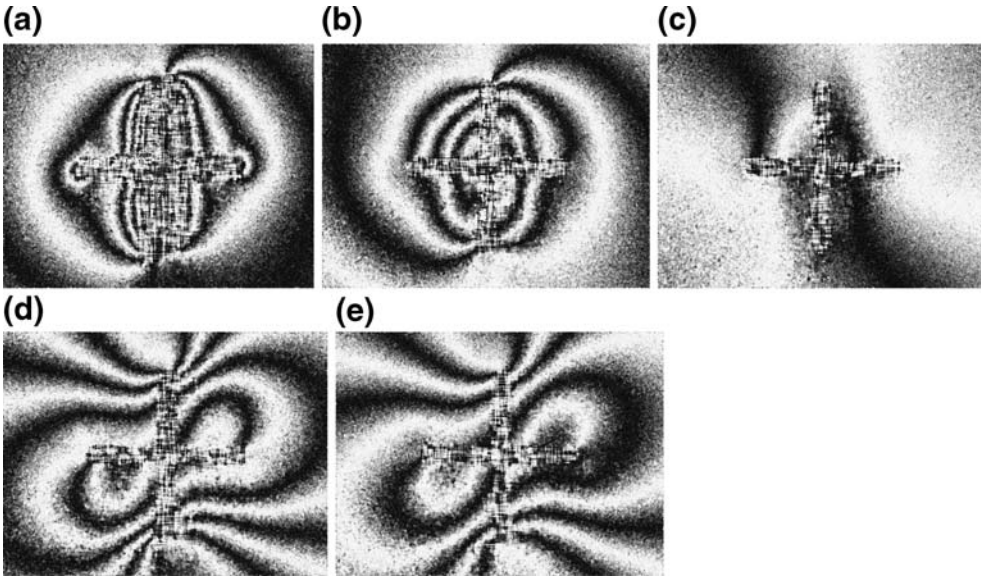

Fig. 8 Incremental fringes measured in sensitivity direction 1: (**a**) 1st increment, (**b**) 2nd increment, (**c**) 3rd increment, (**d**) 4th increment, (**e**) 5th increment

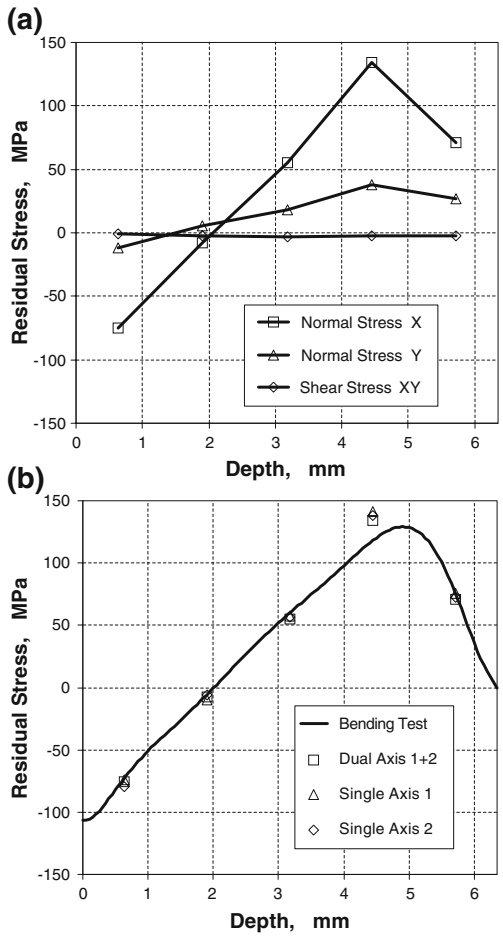

Fig. 9 Residual stress vs. depth profiles computed using dual-axis measurements: (**a**) ESPI in-plane stress results, (**b**) Comparison of σ_x stress from ESPI and bending tests

measurements were done 6 times. All the measurements gave similar results and demonstrated the consistency of the measurements.

Figure 9(b) shows a comparison of the dual-axis ESPI measurements and the stresses evaluated during the bending test. The measured and expected stresses closely agree. The similarity of the stress values computed from single-axis and dual axis data shows that the fringe images obtained in these measurements are mutually consistent. This is an encouraging sign that the measurements and calculations are working well. The dual-axis calculations often give stress results between the results computed from the two single axes. However, this is not always so, for example, the dual-axis calculated stress for the fourth increment in Fig. 9(b) is closer to the expected curve than either of the associated single-axis results. Although not apparent from the graphical presentation, it happens that all the dual-axis measurement results in Fig. 9(b) fall closer to the expect stress curve than the corresponding single-axis results.

The benefit of the dual-axis ESPI technique can be seen more clearly in Fig. 10, which shows the computed shear stress profiles drawn to a much larger scale than in Fig. 9. The shear stresses are expected to be zero at all depths because of symmetry. The shear stresses computed from the single-axis measurements substantially oscillate around zero, but the dual-axis results remain stable and small at all depths.

Discussion

The cross-slitting method can be considered to be a variant of the hole-drilling method with a different shape “hole.”

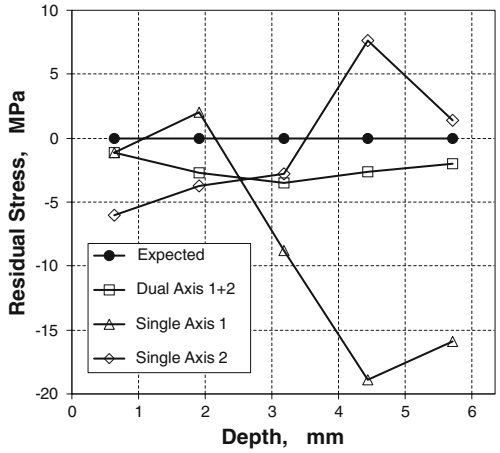

Fig. 10 Shear stress profiles from single-axis and dual-axis measurements

The surface displacements have the same general response to sub-surface stresses, with greatest sensitivity to near-surface stresses and diminishing sensitivity to deeper stresses. For conventional hole-drilling, the stress sensitivity extends to a depth equal to about half the hole diameter. For cross-slitting, the analogous depth dimension is half the slit length. The main advantage of cross-slitting is that it requires removal of much less material. After cutting, there remain four large areas of highly deformed material around the intersection of the cross-slit. These areas provide high-sensitivity data for the inverse calculation in Equation (8), thereby improving computational stability. In addition, the reduced volume of chips produced during cutting is beneficial because these chips tend to scratch the specimen surface as they exit the cut, and impair the ESPI measurements.

The measured stress profile shown in Fig. 9(b) is computed directly from equation (8), without any regularization (a form of smoothing) [18]. Stress profiles of similar smoothness can be achieved from conventional hole-drilling measurements, but they typically require additional regularization. Stress solution stability decreases when a greater number of small depth increments are used. Thus, it is possible that in that case some modest regularization could be required with cross-slitting, but still less than with similar conventional hole-drilling. Since all smoothing processes involve controlled computational distortion, minimizing or removing the need for regularization is a desirable feature.

The combination of data from dual measurement directions increases the measurement and computation burden compared with a single axis measurement. However, care was taken to minimize this burden in both the mechanical design of the apparatus illustrated in Fig. 4 and the associated computations. A particular feature of the apparatus design is the use of a single camera with the multiple beams. Thus, the pixels in all measured images are similarly arranged, with no cross-registration of pixels between multiple cameras required.

Equation (7) shows that the use of dual-axis data adds about 50% to the size of the required calculations. With modern computers, this is not an excessive burden. The computations to give the stress profile results in Fig. 9 took approximately 20 s using a low-end desktop computer. The additional time to collect the second axis images is negligible because most of the overall experiment time is consumed in the slit cutting. Given these modest increased costs, the improved accuracy achievable with dual-axis measurements, as exemplified in Fig. 10, is a practical and useful advance. Correlation of the two single-axis measurements can provide important capabilities for data consistency checking. This will be explored further in subsequent work.

Conclusions

Cross-slitting has been demonstrated to be an effective and accurate alternative to hole-drilling as a method for measuring in-plane residual stresses and their variation with depth. The use of cross-slits enables all three in-plane stress components to be evaluated. The cross-slit geometry has the advantage over a circular hole that it leaves available for ESPI measurements four substantial areas of highly deformed material adjacent to the cross-slits. These areas provide a rich data source for the residual stress calculations, thereby enhancing evaluation accuracy. In addition, the cutting of cross-slits removes much less material than from an equivalent circular hole. This feature reduces the volume of chips produced and minimizes the occurrence of surface damage as the chips exit the cut.

A dual-axis ESPI system has been developed that removes the directional bias inherent in a conventional single-axis system. The additional data from the second axis enriches the available data pool, and thereby enhances the measurement accuracy. This benefit is not limited to the use of cross-slits, and could also be gained when using the hole-drilling technique. With organized arrangement of the data handling, the residual stress evaluations from dual-axis data are only about 50% more demanding than an equivalent single axis calculation, and can be done quite compactly with an ordinary desktop computer.

Acknowledgments This work was financially supported by the Natural Science and Engineering Research Council of Canada (NSERC).

References

1. ASTM (2008) Determining residual stresses by the hole-drilling strain-gage method. ASTM standard test method E837-08. American Society for Testing and Materials, West Conshohocken
2. Schajer GS (1996) Hole-drilling and ring core methods. In: Lu J (ed) Handbook of measurement of residual stresses, Chapter 2. Fairmont, Lilburn, pp 5–20
3. Jones R, Wykes C (1989) Holographic and speckle interferometry. Cambridge University Press, Cambridge
4. Sirohi RS (1993) Speckle metrology. Marcel Dekker, New York
5. Nelson DV, McCrickerd JT (1986) Residual-stress determination through combined use of holographic interferometry and blind-hole drilling. Exp Mech 26(4):371–378
6. Steinzig M, Ponslet E (2003) Residual stress measurement using the hole drilling method and laser speckle interferometry—Part I. Exp Tech 27(3)
7. Cheng W, Finnie I (2007) Residual stress measurement and the slitting method. Springer, New York
8. Prime MB (1999) Residual stress measurement by successive extension of a slot: the crack compliance method. Appl Mech Rev 52(2):75–96
9. Cloud GL (1995) Optical methods of engineering analysis. Cambridge University Press, Cambridge
10. Malacara D, Servín M, Malacara Z (2005) Chapter 6: Phase-detection algorithms, 2nd edn. Taylor & Francis, Boca Raton
11. Giglia DC, Pritt MD (1998) Two-dimensional phase unwrapping: theory, algorithms, and software. Wiley-Interscience, New York
12. Schajer GS, Prime MB (2006) Use of inverse solutions for residual stress measurements. ASME Journal of Engineering Materials and Technology 128(3):375–382
13. Montay G, Sicot O, Maras A, Rouhaud E, François M (2009) Two dimensions residual stresses analysis through incremental groove machining combined with electronic speckle pattern interferometry. Exp Mech 49(4):459–469
14. Parker RL (1994) Geophysical inverse theory. Princeton University Press, New Jersey
15. ANSYS® Inc (2009) Ansys finite element software. Canonsburg.
16. Mayville RA, Finnie I (1981) Uniaxial stress-strain curves from a bending test. Exp Mech 22(6):197–201
17. Schajer GS, An Y (2009) Inverse calculation of uniaxial stress-strain curves from bending test data. J Eng Mater Technol 131(4)
18. Tikhonov A, Goncharsky A, Stepanov V, Yagola A (1995) Numerical methods for the solution of ill-posed problems. Kluwer, Dordrecht